[Article ID] 1003- 6326(2002)04- 0695- 07

Macro- and microstructural changes in hydrogenated $TiMn_2$ and Ta①

S. Semboshi, N. Masahashi, S. Hanada
(Institute for Materials Research, Tohoku University, Sendai 980-8577, Japan)

[Abstract] Binary $TiMn_2$ alloys with various compositions were arc melted in an Ar atmosphere. These alloys consist of $TiMn_2$ and a small amount of TiMn depending on alloy composition. Annealed Ti-59.4%Mn exhibits the greatest capacity for hydrogen absorption and the smallest degradation of capacity during repeated hydrogen absorption and desorption. No apparent macro- and microstructural changes are observed in Ti-59.4%Mn by repeated hydrogenation of 30 cycles. At Mn content higher than 59.4%Mn, the formation of nano-sized Ti-hydride and the lattice expansion due to retained interstitial hydrogen were confirmed in repeatedly hydrogenated alloys. Pulverized powders were refined in all the alloys with increasing the number of repeated hydrogenation cycles. Many onion-like cracks are introduced in annealed pure Ta with 100 μm equiaxed grains by holding at 1473 K followed by furnace cooling to room temperature in a hydrogen atmosphere, but no crack is observed after holding at 1473 K in a hydrogen atmosphere followed by furnace cooling in an Ar atmosphere. It is concluded that the surface activation is attained in a hydrogen atmosphere at 1473 K and multiple cracking occurs by absorbing a large amount of hydrogen at lower temperature. Volume expansion and dislocations generated by hydrogenation and hydride formation are responsible for multiple cracking. Hydrogen-induced multiple cracking in Ta occurs in the following sequence: hydrogen absorption, lattice expansion, hydride formation, and crack nucleation and propagation. Powder fabrication of Ta by hydrogenation is discussed in comparison with the hydrogen pulverization of intermetallic alloys.

[Key words] macrostructure; microstructure; hydrogen absorbing alloy
[CLC number] TG 139.7 [Document code] A

1 INTRODUCTION

It is well known that macro- and microstructures of hydrogen absorbing metals or alloys are remarkably changed by absorbing hydrogen. Macroscopically, some bulk alloys are readily broken into small chips or pieces when the alloys are exposed to a hydrogen atmosphere. Recent studies have demonstrated that fine refractory alloy powders can be fabricated by hydrogenation without applying mechanical stress if alloy system, composition, microstructure and processing condition are controlled[1~4]. By further controlling the above conditions more strictly, alloy powders will be produced in a intended size. This hydrogen pulverization process is considered to be very promising to produce clean and low cost alloy powders, compared to other powder fabrication processes such as a gas atomization process and a plasma rotating electrode process. This is because contamination from an atmosphere or a nozzle is inevitable in the gas atomization process, and fine powders are not obtained and in addition the preparation of an electrode is not so easy in the plasma rotating electrode process. At present a mechanism for the hydrogen pulverization is not well understood. If the pulverization can be freely controlled on the basis of the mechanism clarified, the hydrogen pulverization process will be applied to many metals and alloys for powder fabrication.

Microscopically, a large amount of hydrogen absorption in some metal and alloys creates fine hydride particles and introduces dislocations arising from lattice expansion. These microstructural changes often degrade the hydrogen absorbing properties in hydrogen storage alloys used industrially. Moreover, hydrogen absorption and desorption cycles in industrial uses result in further refinement of powders, which also leads to degradation of hydrogen absorbing properties accompanied by cyclic hydrogenation. If the microstructural changes during cyclic hydrogenation can be controlled, the degradation of hydrogen absorbing properties will be suppressed or alleviated.

In view of the above background we have investigated macro- and microstructural changes in hydrogenated $TiMn_2$ and pure Ta in this study. $TiMn_2$ is selected to obtain some information for improving hydrogen absorbing properties, since $TiMn_2$ base multi-component alloys are industrially used as hydrogen storage alloys. Pure Ta is selected to develop a new powder fabrication process by using hydrogen pulverization, since its fine powder supplied by another method is now widely used in capacitors.

① [Received date] 2001- 10- 08

2 EXPERIMENTAL

According to the Ti-Mn binary phase diagram in Fig. 1, C14-type $TiMn_2$ intermetallic compound exists in the composition range approximately between 60% and 70% Mn (mole fraction)[5]. Binary $TiMn_2$ base alloys with nominal compositions of Ti-(56, 57, 59, 60, 61, 62, 64, 67)% Mn (mole fraction) were arc-melted four times to attain compositional homogeneity in an Ar atmosphere, using 99.99% Ti and 99.9% Mn as raw materials. The arc melted buttons were homogenized at 1 323 K for 72 h in a quartz tube evacuated and filled with Ar. Inductively coupled plasma (ICP) analysis was carried out to determine the compositions of the alloys. Optical microscopy (OM), scanning electron microscopy (SEM), energy dispersive spectroscopy (EDS), transmission electron microscopy (TEM) and X-ray diffractometry (XRD) were employed to investigate the constituent phases, compositions, microstructures and lattice constants. A commercially pure Ta (99.996%) plate with 6 mm in thickness was cold rolled to 1 mm thick plate and electro-discharge machined into disks with 5 mm in diameter. These disks were annealed in vacuum at 1 773 K for 6 h to obtain recrystallized grains. Hydrogenation was carried out in Sieverts-type apparatus and a vacuum furnace in a hydrogen atmosphere.

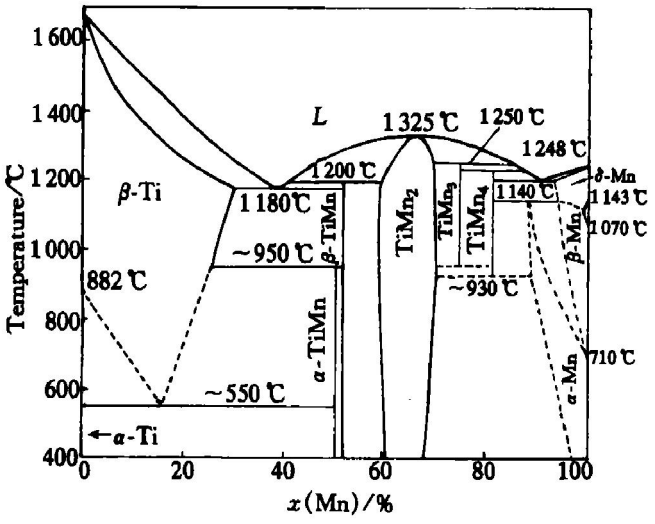

Fig. 1 Ti-Mn binary phase diagram

3 RESULTS AND DISCUSSION

3.1 Binary $TiMn_2$ alloys

ICP analysis indicated that the annealed binary alloys have the compositions of 56.4%, 57.3%, 59.4%, 59.8%, 61.2%, 62.0%, 64.0% and 66.8% Mn. These analyzed compositions will be used hereafter in this paper instead of the nominal compositions. All the homogenized alloys were found to consist of $TiMn_2$ with a small amount of TiMn in spite of the homogenization treatment, suggesting that the decomposition of TiMn was very sluggish. Fig. 2 shows composition dependence of volume fraction of $TiMn_2$ phase. This indicates that the compositions determined by ICP do not correspond to those of $TiMn_2$ phase. The compositions of $TiMn_2$ phase determined by SEM-EDS are plotted in Fig. 3 against the compositions determined by ICP. It is evident from Fig. 3 that Mn content in $TiMn_2$ phase is almost constant (60.2%, mole fraction) up to alloy composition of Ti-59.4% Mn and increases rapidly with increasing alloy composition. This result seems to be consistent with the phase diagram in Fig. 1. That is, $TiMn_2$ and TiMn are equilibrated at a fixed composition for each phase at compositions with Mn content lower than about 60%, while Mn content in $TiMn_2$ increases with increasing Mn content of the alloys in the single phase $TiMn_2$ range.

Fig. 4 shows pressure—composition (PC)

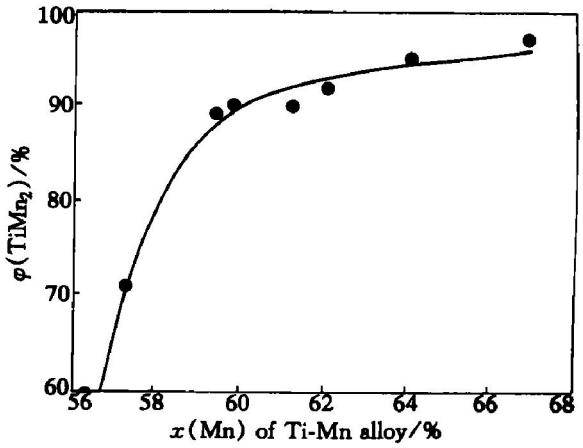

Fig. 2 Composition dependence of volume fraction of $TiMn_2$ phase

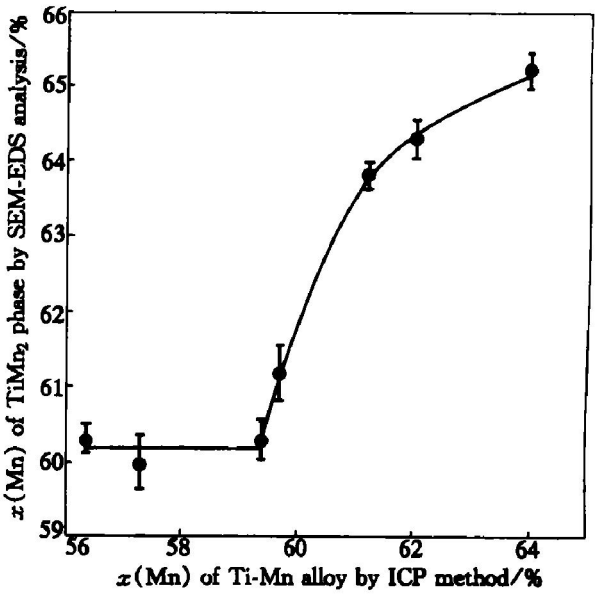

Fig. 3 Relationship between Mn content of Ti-Mn alloys by ICP and that of $TiMn_2$ phase by SEM-EDS

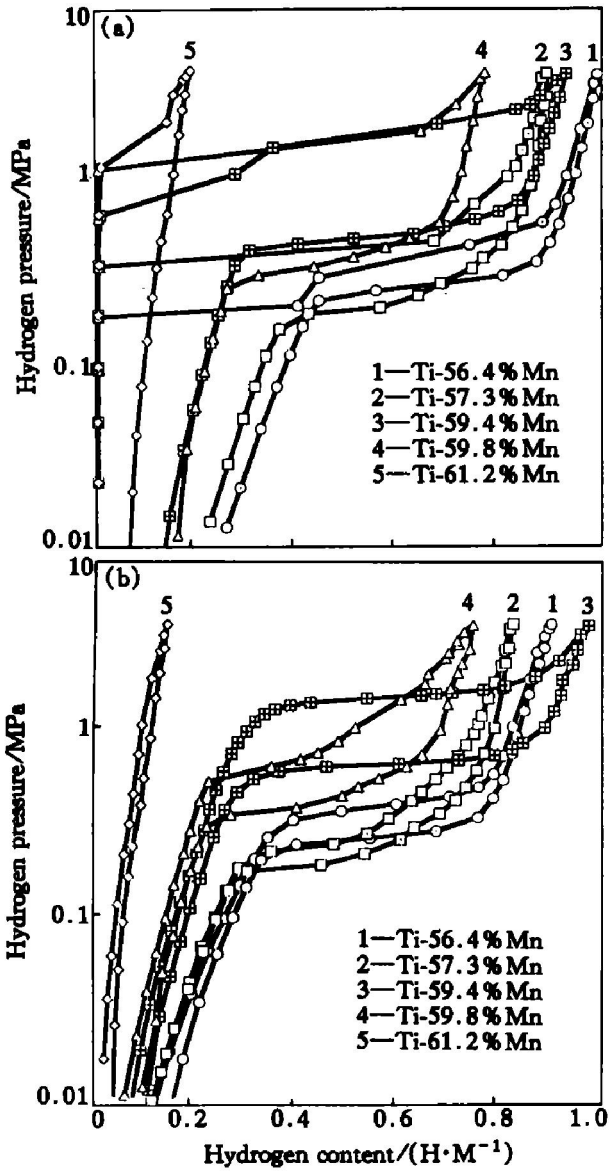

Fig. 4 PC curves of annealed Ti-Mn alloys
(a) —1st cycle; (b) —2nd cycle

isotherms of $TiMn_2$ binary alloys. For the PC curve measurements alloy buttons were crushed into chips or blocks with sizes of about 1 mm in a glove box under an Ar atmosphere and mounted in a sample holder of Sieverts-type apparatus without exposure to air. PC curves were measured repeatedly at room temperature by changing hydrogen pressure from 0.01 to 3.2 MPa. Fig. 4(a) and (b) show the results for the first and second cycle, respectively. It is found that hydrogen absorbing capacity is very sensitive to alloy composition and some alloys in Fig. 4(a) exhibit an abrupt increase in hydrogen content at an initial stage of the PC curve. This increase is due to pulverization of coarse particles. In the second cycle the PC curve is smoothly drawn, as can be seen in Fig. 4(b). Strictly speaking, therefore, Fig. 4(a) does not denote true PC curves, because the hydrogen content during the measurement does not reach the equilibrium value in the center of such coarse particles, but in this paper we call a hydrogen absorption —desorption curve by a PC curve for convenience to discuss the hydrogen absorbing capacity on the basis of PC curves. Fig. 5 shows hydrogen content in the alloys at a hydrogen pressure of 3.2 MPa as a function of Mn content of the alloys determined by ICP. Hydrogen content has a maximum of 1.0 H/M at Ti-59.4% Mn. With decreasing Mn content hydrogen content decreases slightly. As shown in Figs. 2 and 3, in the composition range between 56.4% to 59.4% Mn, the volume fraction of $TiMn_2$ with the constant composition of 60.2% Mn increases with increasing Mn content, thereby leading to the increase of hydrogen absorbing capacity. In the composition range between 59.4% to 66.8% Mn, with increasing Mn content in the alloys, Ti content in $TiMn_2$ decreases, although the volume fraction of $TiMn_2$ phase increases. This decrease is attributable to the rapid decrease in hydrogen absorbing capacity in Fig. 5.

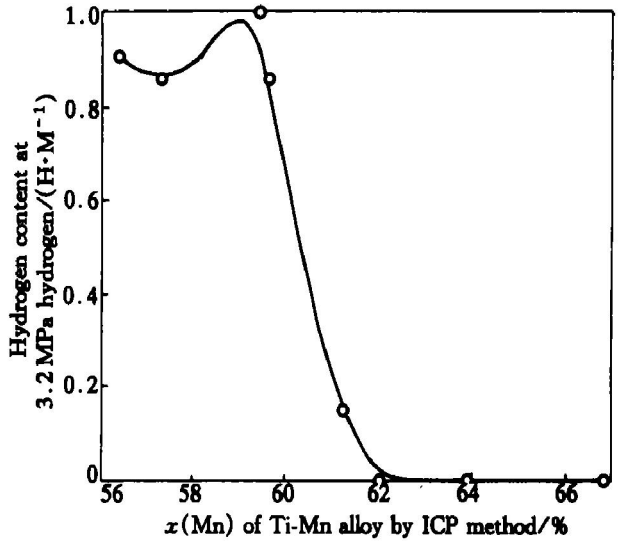

Fig. 5 Composition dependence of hydrogen content at hydrogen pressure of 3.2 MPa

Fig. 6 shows hydrogen content in the alloys at a hydrogen pressure of 3.2 MPa as a function of hydrogenation cycle. The hydrogen content at the hydrogen pressure of 3.2 MPa decreases with increasing number of hydrogenation cycles. The degradation caused by cyclic hydrogenation is more significant in Ti-59.8% Mn than in Ti-59.4% Mn. XRD analysis indicates clearly that Ti-hydride (δ-TiH) appears in 30 cycles-hydrogenated Ti-59.8% Mn, as shown in Fig. 7. Correspondingly, hydrogen content in Ti-59.8% Mn was found to increase from 0.001% H (mass fraction) before hydrogenation to 0.672% H (mass fraction) after 30 cycles hydrogenation. XRD analysis also indicated an increase in lattice parameter of 30 cycles-hydrogenated Ti-59.8% Mn. Thus, the increased residual hydrogen content after 30 cycles hydrogenation contributes to both Ti-hydride formation and lattice expansion. In contrast, no apparent change was found in 30 cycles-hydrogenated Ti-

59.4% Mn. Macro- and microstructural changes were observed to investigate a mechanism of the degradation. Macrostructural changes of particle size by cyclic hydrogenation are shown in Fig. 8. Since the average size of initial particles is about 1 mm, pulverization is seen to occur abruptly during the first hydrogenation cycle. Further refinement by cyclic hydrogenation is not so significant. Hydrogen pulverization has been reported in some two phase alloys consisting of brittle intermetallic(s). As pointed out in Ref. [1~4], the stress induced by lattice expansion due to hydrogen absorption would produce cracks at a brittle intermetallic which is needed to be at least one of constituent phases. The present alloy is composed of brittle $TiMn_2$ and TiMn and hence the stress induced by hydrogen absorption creates cracks readily in the intermetallics or at the interface between the intermetallics. Also, the Ti-hydride is formed in the present alloy. Crack nucleation will become easy at Ti-hydride particles.

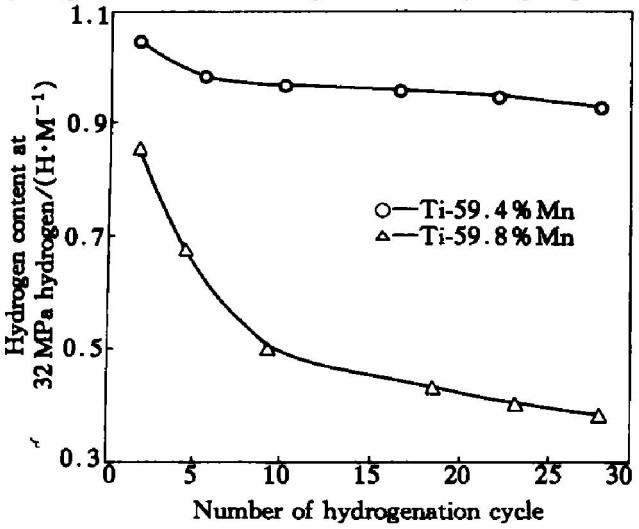

Fig. 6 Hydrogen content at hydrogen pressure of 3.2 MPa as a function of hydrogenation cycle

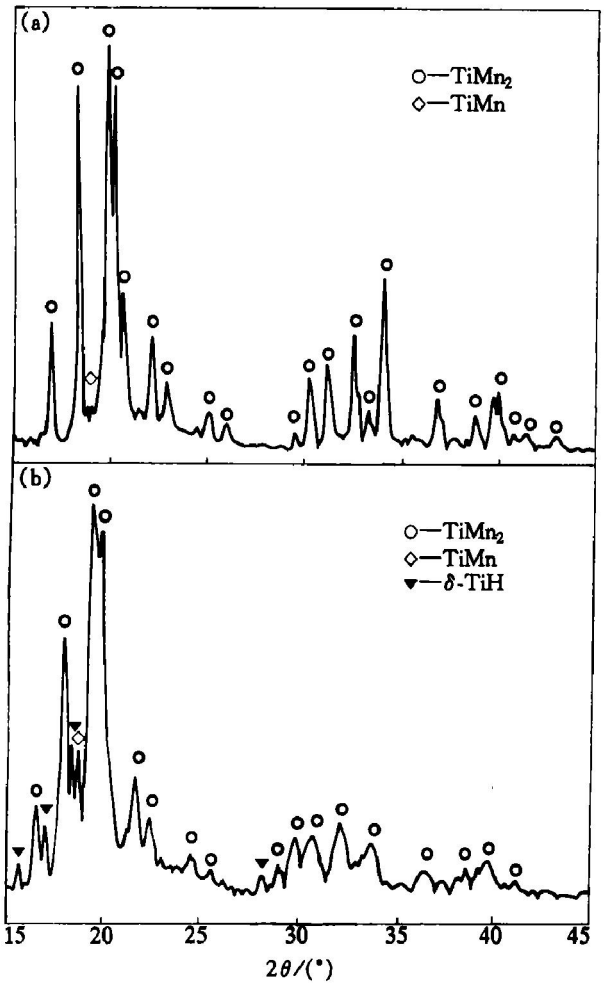

Fig. 7 X-ray diffraction patterns of Ti-59.8% Mn alloy
(a) —As-annealed; (b) —30 cycles hydrogenated

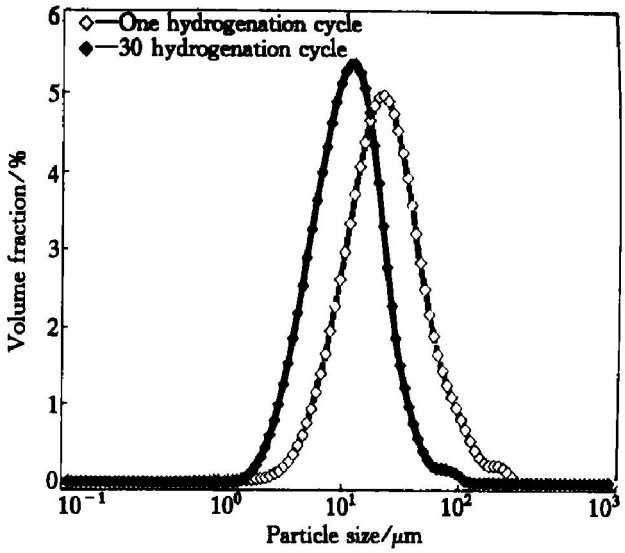

Fig. 8 Particle size distribution of Ti-59.8% Mn alloy after one and 30 cycles hydrogenation

Fig. 9 shows high resolution (HRTEM) micrographs of $TiMn_2$ with the associated electron diffraction patterns for one cycle-hydrogenated (a) and 30 cycles-hydrogenated (b) Ti-59.8% Mn. It should be noted that homogeneous lattice image with a constant spacing was observed in $TiMn_2$ before hydrogenation, and in TiMn before and after hydrogenation. After one hydrogenation cycle, nano-sized (~5 nm) regions with Moire patterns are observed as shown in Fig. 9(a), where typical regions are marked with circles. No diffraction spot other than from $TiMn_2$ is observed in the associated diffraction pattern. After 30 hydrogenation cycles nano-sized regions with Moire patterns are more clearly recognized, as shown in Fig. 9(b) and both diffraction spots from $TiMn_2$ and Debye rings are visible. The nano-sized regions with random orientations are observed more frequently after 30 cycles than one cycle, although the size is not significantly changed. Precise measurement of distances between (000) and Debye rings revealed that the rings correspond to the formation of δ-TiH, indicating that the nano-sized regions observed in Fig. 9(a) also correspond to δ-TiH, in spite of the lack of corresponding spectra in the XRD pattern and

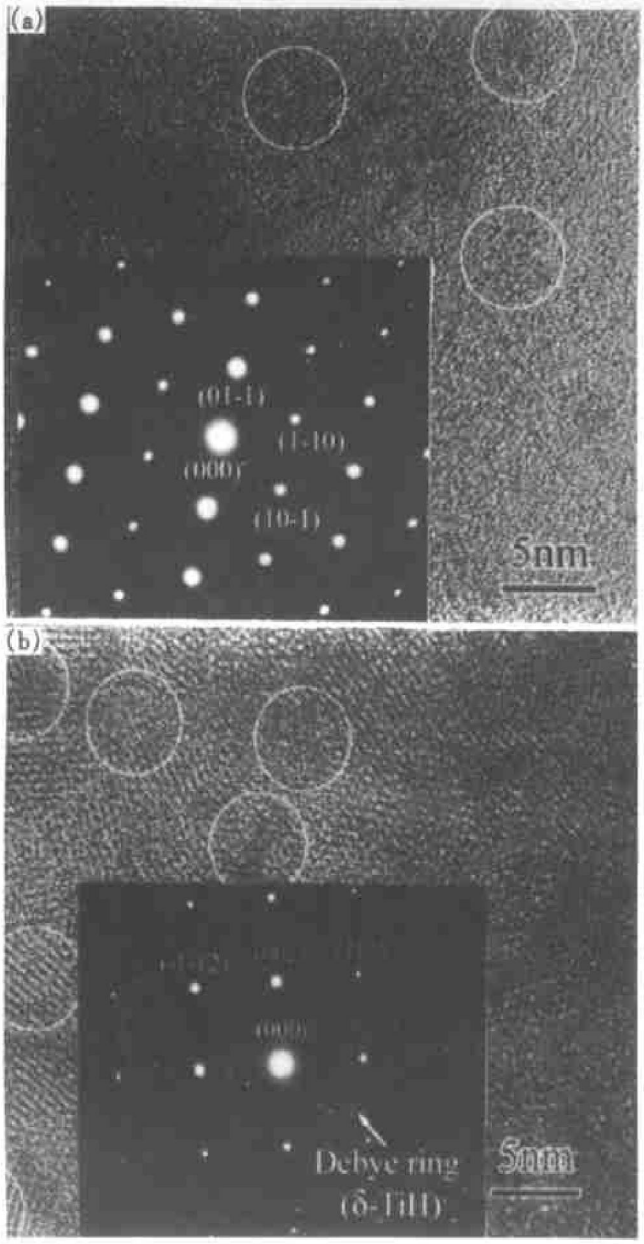

Fig. 9 HRTEM micrographs and diffraction patterns of $TiMn_2$ in Ti-59.8% Mn
(a) —After one cycle hydrogenation;
(b) —After 30 cycles hydrogenation

selected area diffraction in TEM, probably due to the small fraction[6].

Degradation of hydrogen absorbing capacity accompanied by cyclic hydrogenation is a fatal issue in applications of hydrogen absorbing alloys. In this experiment, it is confirmed that cyclic hydrogenation causes lattice expansion and δ-TiH formation. Correspondingly, the hydrogen absorbing capacity is found to decrease remarkably with increasing number of hydrogenation cycles. Therefore, the degradation of hydrogen absorbing capacity should be explained by considering these changes induced by cyclic hydrogenation. The degradation has been usually discussed in terms of pulverization, impurity gas contamination, or transformation to another phase. Among them, pulverization is known to result usually in a decrease of thermal conductivity, thereby reducing the reactivity of hydrogen with the alloy. However, the cyclic hydrogenation in this study was performed by changing hydrogen pressure at room temperature. Therefore, the decrease of thermal conductivity will be ruled out in discussion of the degradation. Impurity gas contamination can also be ruled out, because we used very high purity hydrogen, and hydrogenation was conducted in Sieverts-type equipment without exposure to air. Therefore, we will consider the phase transformation as a result of hydrogen absorption. As mentioned above, two types of changes, lattice expansion and δ-TiH formation are caused during hydrogenation. These changes induced by cyclic hydrogenation, leading to degradation of hydrogen absorbing capacity, seem to be inevitable in this alloy. Evidently, a small amount of "trapped" hydrogen, which cannot be desorbed from samples by lowering the hydrogen pressure to 0.01 MPa, plays an important role in the degradation. To clarify a mechanism of the degradation, further detailed HRTEM observations of the formation sequence for nano-sized regions are needed in relation to retained hydrogen content.

3.2 Pure Ta

A recent study on hydrogenation of Ta-Ni alloys has shown that two phase alloys consisting of Ta-Ni BCC solid solution and Ta_2Ni phase with C16-type Laves structure are pulverized by hydrogenation, while a single phase Ta-Ni solid solution is not[7]. The hydrogenation in the experiment was carried out by arc melting in an Ar+ 5% H_2 atmosphere and then holding in pure H_2 at room temperature without exposure to air. In addition, XRD analysis after the pulverization indicated the lattice expansion of Ta-Ni solid solution by hydrogen absorption. It was concluded from these results that crack initiation occurs at a brittle Ta_2Ni phase by stress concentration due to the lattice expansion, which leads to further enhancement of hydrogen absorption through fresh crack surfaces and to acceleration of pulverization. If this is the case, the existence of a brittle phase is a prerequisite to pulverize an alloy, along with the existence of a phase absorbing a large amount of hydrogen. A preliminary experiment indicated that pure Ta was not pulverized by the convenient hydrogenation method of arc melting in an Ar+ 5% H_2 atmosphere followed by holding at room temperature in an hydrogen atmosphere. This result is consistent with the above conclusion, since no brittle second phase is included. Then, we consider whether hydride formed by hydrogen absorption acts as a brittle second phase for pulverization. According to the Ta-H phase diagram[8], a large amount of hydrogen becomes soluble in α-Ta with decreasing temperature and ε-hydride forms below 334 K. Hydrogenation of Ta was carried out, referring to the phase diagram. First, Ta disks were heated at a heating rate of 20 K/min to 673, 1073

and 1 473 K, held for 3 h and then furnace cooled to room temperature. All these treatments were performed under a hydrogen pressure of 0.1 MPa. After the hydrogenation treatments no change was observed in the disks heated to 673 and 1 073 K, while many cracks were introduced in the Ta disk heated to 1 473 K. Fig. 10 shows the appearance of hydrogen-induced cracks. One can see onion-like cracks in Fig. 10 (a) at a low magnification by OM and transgranular cracks in Fig. 10(b) at a high magnification by SEM. In addition to the cracks straight bands like deformation bands or twins are occasionally seen in Fig. 10(b). They appear to be parallel to some crystallographic directions. TEM observation revealed that hydrogenated Ta contains a high density of dislocations, implying that the straight products are deformation bands. Detailed analysis is underway at present. Fractography revealed that pseudo-cleavage fracture is dominant. This observation means that mechanical properties of Ta is drastically changed by hydrogen absorption.

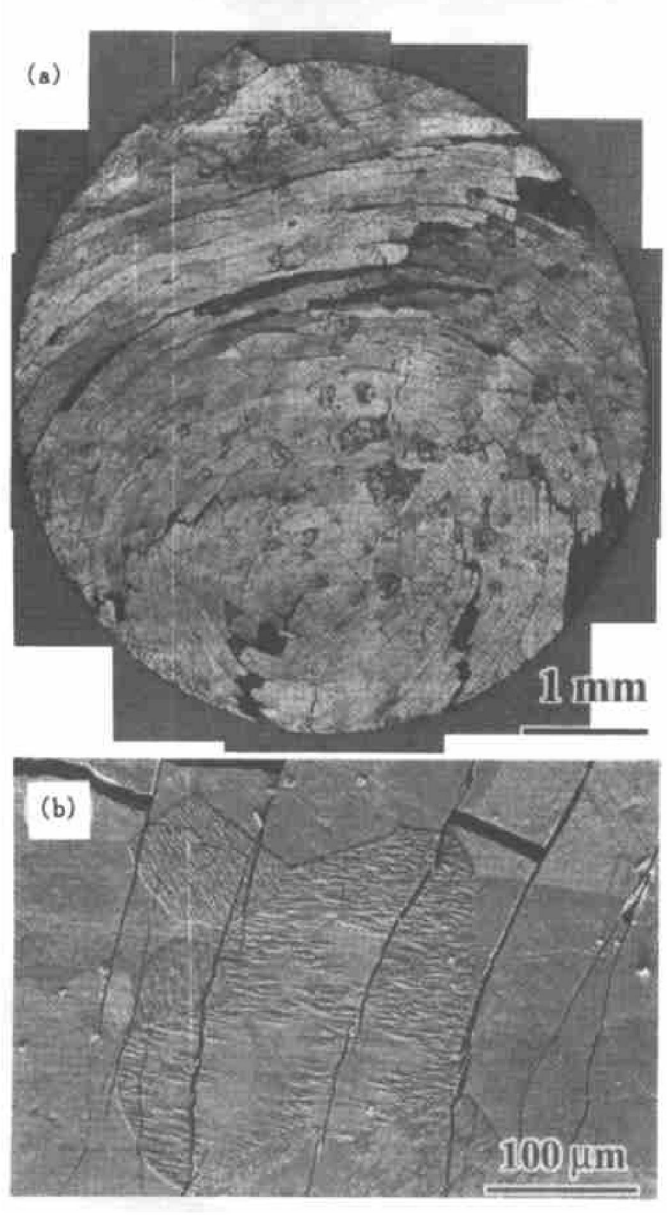

Fig. 10 Hydrogenation-induced cracks in tantalum
(a) —OM image; (b) —SEM image

Next, after holding a Ta disk at 1 473 K for 3 h under a hydrogen pressure of 0.1 MPa, hydrogen was replaced by Ar and the Ta disk was held for 1 h, and then furnace cooled in Ar to room temperature. Referring to the Ta-H phase diagram, approximately 40%H is soluble in Ta at 473 K, although the solubility limit of hydrogen in Ta appears to be less than a few mole fraction at 1 473 K. Hence, hydrogen content in a Ta disk will not increase when the disk is cooled in an Ar atmosphere after holding in a hydrogen atmosphere at 1 473 K. Indeed, no cracking was observed in the disk which was cooled in Ar after holding in H_2 at 1 473 K. On the other hand, cracks were introduced more significantly when a Ta disk was held at 1 473K for 3 h under a hydrogen pressure of 0.1 MPa, held at 473 K for 1 h in the same hydrogen atmosphere, and then cooled to room temperature in an Ar atmosphere, as compared to the disk furnace cooled from 1 473 K to room temperature in H_2 (as shown in Fig. 10). Hydrogen content would be higher in the former disk than in the latter. XRD analysis of the former disk indicated that the lattice constant of hydrogenated Ta increases by 3.7% after the above hydrogenation treatment, which corresponds to volume expansion by 11.4%. These results evidence that a large amount of hydrogen is absorbed during cooling from 1 473 K or holding at 473 K in a hydrogen atmosphere, and the absorbed hydrogen is not desorbed during cooling from 473 K in Ar. The stress caused by lattice expansion due to hydrogen absorption is, therefore, responsible for hydrogen-induced cracking. Since ε-hydride is stable below 334 K[8], absorbed hydrogen atoms at 473 K are located at interstitial lattice sites without forming ε-hydride. In order to investigate whether the hydrogen-induced cracking occurs during holding at 473 K or during cooling from 473 K, in other words whether ε-hydride formation is concerned with cracking, a Ta disk was held at 473 K for 1 h in H_2 after holding at 1 473 K for 3 h in H_2, and then heated to 1 073 K in vacuum for dehydrogenation. No hydrogen cracking was induced after this heat treatment in vacuum. Instead, band-like products similar to the products in Fig. 10(b) were densely distributed near disk surfaces. This observation clearly indicates that the band-like products, which are generated at 473 K in H_2, do not induce hydrogen cracking, but cracking is accompanied by ε-hydride formation as well as lattice expansion due to hydrogen absorption. It is concluded, therefore, that hydrogen cracking of pure Ta is caused by holding at high temperature for surface activation, large lattice expansion for stress concentration and ε-hydride formation for crack nucleation. Thus, the controlled hydrogenation described above is

found to break pure Ta disks into small chips or pieces which are very fragile.

4 CONCLUSIONS

1) Hydrogen absorbing capacity in binary $TiMn_2$ alloys exhibits a peak at Ti-59.4%Mn, and its degradation by hydrogen absorption and desorption cycles between 0.01 to 3.2MPa hydrogen takes place slightly. No apparent microstructural change is observed in the repeatedly hydrogenated Ti-59.4%Mn.

2) When Mn content is slightly increased the hydrogen absorbing capacity decreases rapidly with increasing hydrogenation cycle. Correspondingly, nano-sized hydride particles and lattice expansion are retained.

3) Hydrogen-induced cracking in pure Ta is caused by surface activation at 1473K to remove oxide film, a large amount of hydrogen absorption at 473K to induce high stress due to lattice expansion, and hydride formation below 334K to introduce crack initiation sites.

[REFERENCES]

[1] Semboshi S, Tabaru T, Hosoda H, et al. Effect of microstructure on hydrogen pulverization of Nb_3Al/Nb two phase alloys [J]. Intermetallics, 1998, 6: 61- 69.

[2] Hosoda H, Tabaru T, Semboshi S, et al. Hydrogen absorption of Nb-Al alloy bulk specimens [J]. J Alloys and Compounds, 1998, 281: 268- 274.

[3] Kosuge M, Hosoda H, Hanada S. Preparation of Nb-Cr alloy powder by hydrogenation [J]. J Japan Inst Metals, 1998, 62: 681- 689.

[4] Sugiyama T, Hosoda H, Hanada S. Effect of volume fraction of constituent phases, lattice strain and mechanical properties on the hydrogen pulverization of Nb-Cr-Ti intermetallic alloys [J]. J Japan Inst Metals, 1999, 63: 1535- 1544.

[5] Murray J L. Binary Alloy Phase Diagrams [M]. Murray J L, Bennet L H, Baker H. American Society for Metals, 1987, 2: 1592.

[6] Semboshi S, Masahashi N, Hanada S. Degradation of hydrogen absorbing capacity in cyclically hydrogenated $TiMn_2$[J]. Acta mater, 2001, 49(5): 927- 935.

[7] Semboshi S, Masahashi N, Hanada S. Hydrogen pulverization in intermetallic-based alloys [A]. Schneibel J H, Hemker K J, Noebe R D, et al. Mat Res Soc Symp Proc [C]. MRS Pennsylvania, 2001. 1- 6.

[8] Scober T, Bozic D. A revision of the Ta-H phase diagram [J]. Scripta Metallurgica, 1977, 11: 397- 400.

(Edited by YANG Bing)